UNIVERSITY OF AMSTERDAM

UvA-DARE (Digital Academic Repository)

Quantitative and localized spectroscopy for non-invasive bilirubinometry in neonates

Bosschaart, N.

Publication date
2012

[Link to publication](#)

CHAPTER 5

Measurements of wavelength dependent scattering and backscattering coefficients by low-coherence spectroscopy

Quantitative measurements of scattering properties are invaluable for optical techniques in medicine. However, non-invasive, quantitative measurements of scattering properties over a large wavelength range remain challenging.

We introduce low-coherence spectroscopy (LCS) as a non-invasive method to locally and simultaneously measure scattering μ_s *and* backscattering μ_b coefficients from 480 to 700 nm with 8 nm spectral resolution. The method is tested on media with varying scattering properties (μ_s = 0.15-34 mm^{-1} and μ_b = 2.10^{-6}–2.10^{-3} mm^{-1}), containing different sized polystyrene spheres. The results are in excellent agreement with Mie theory.

5.1   Introduction

Quantitative determination of the optical properties of tissue is invaluable in biomedical optics. The majority of optical diagnostic techniques rely on the spectral absorption and scattering properties of tissue, which provide information on its composition and structure. The same optical properties are of essential importance for the development and optimization of optical therapeutic techniques. However, despite the existence of many spectroscopic methods it is still a challenge to do non-invasive, quantitative measurements of the absorption and scattering properties *in vivo* over a large wavelength range.

In Chapter 4, we introduced low-coherence spectroscopy (LCS) to do quantitative and localized measurements of absorption coefficients $\boldsymbol{\mu_a}$ over a wavelength range of 480-700 nm with a spectral resolution of 8 nm [1] (all wavelength dependent parameters in this Chapter will be denoted by a boldfaced character). In this Chapter, we use LCS to quantitatively and simultaneously measure scattering $\boldsymbol{\mu_s}$ and backscattering $\boldsymbol{\mu_b}$ coefficients on a wide range of scattering media ($\boldsymbol{\mu_s}$ = 0.15-34 mm^{-1} and $\boldsymbol{\mu_b}$ = 2.10^{-6}–2.10^{-3} mm^{-1}). Thereby, we demonstrate new opportunities for non-invasive scattering property measurements. *In vivo* measurements of the quantitative value of $\boldsymbol{\mu_s}$ and $\boldsymbol{\mu_b}$ can assist in differentiating between tissue types [2] and modeling of light-tissue interactions. The spectrally resolved information of $\boldsymbol{\mu_s}$ and $\boldsymbol{\mu_b}$ gives additional valuable information: e.g. the power dependency of $\boldsymbol{\mu_s}$ on wavelength and wavelength dependent oscillations in $\boldsymbol{\mu_b}$, which have shown to be related to tissue morphology [3,4].

Whereas extensive research on tissue (back)scattering has been performed in the areas of light scattering spectroscopy (LSS) [3] and angle-resolved low-coherence interferometry [4], these studies lack quantification of $\boldsymbol{\mu_s}$ and $\boldsymbol{\mu_b}$, since their primary aim has been to retrieve the size of the scattering particles. Quantification of $\boldsymbol{\mu_s}$ and $\boldsymbol{\mu_b}$ has been shown in optical coherence tomography studies [2,5], but these studies were limited to the measurement of $\boldsymbol{\mu_s}$ and $\boldsymbol{\mu_b}$ averaged over the bandwidth of the spectrum, i.e. no spectral information was obtained. Moreover, in these studies quantitative agreement with theory is rarely obtained for highly scattering media, due to multiple scattering contributions to the signal [5]. Other (diffuse) reflectance spectroscopy techniques are able to measure $\boldsymbol{\mu_b}$ and the reduced scattering coefficient $\boldsymbol{\mu_s'}$ [7], but this requires additional information on the scattering anisotropy $\boldsymbol{g}$ to obtain $\boldsymbol{\mu_s}$. Thus, compared to the existing methods for scattering property measurements, LCS offers the unique possibility for a combination of simultaneous, quantitative and spectrally resolved measurement of $\boldsymbol{\mu_s}$ and $\boldsymbol{\mu_b}$. These measurements will therefore assist in more complete, and likely more accurate, characterization of the tissue of interest.

Since LCS is a low coherence interferometry technique, another advantage of LCS is the possibility to measure in a controlled and confined volume [2,5,6], which is important when measuring local optical properties in often inhomogeneous tissue. In addition, knowledge of the contribution of scattering to the measured $\boldsymbol{\mu_t}$ is crucial for accurate $\boldsymbol{\mu_a}$ determination, because LCS determines the $\boldsymbol{\mu_a}$ from the total attenuation coefficient $\boldsymbol{\mu_t}$ of the sample. Therefore, this Chapter also provides a more thorough understanding of this contribution.

5.2   Materials and methods

5.2.1   *System and acquisition*

Using LCS, we measured μ_b and μ_s of aqueous non-absorbing suspensions of different sized polystyrene spheres and validated our results with Mie theory. Therefore, we measured back scattered power spectra $S(\ell)$ at controlled geometrical path lengths ℓ of the light in a sample. Our LCS system, which is described in detail in Chapter 4 [1], consists of a Michelson interferometer and is optimized for 480–700 nm. The geometrical roundtrip path length ℓ (ℓ=0–2 mm, with ℓ=0 the sample surface) is controlled by translating the reference mirror, in steps of 27 µm. By translating the sample, focus tracking of the 64 µm^2 spot size (see Section 5.2.3) in the sample is achieved. Around ℓ, the signal is modulated by scanning the piezo-driven reference mirror (23 Hz) resulting in a scanning window of $\Delta\ell \approx 44$ µm and an axial resolution for $S(\ell)$ of $\frac{1}{2}\Delta\ell \approx 22$ µm. The optical power at the sample is 6 mW. A multimode fiber (ø=62.5 µm) guides the reflected light from both arms to a photodiode.

5.2.2   *Determination of μ_s and μ_b*

Signal processing after acquisition, which is described in detail in Chapter 4 [1], results in averaged power spectra $S(\ell)$ with 8 nm resolution (~500 averages per ℓ, to avoid any speckle influences, i.e. spectral modulations on $S(\ell)$ caused by interference between scattering particles). We describe $S(\ell)$ with a single exponential decay model [2]:

$$S(\ell) = S_0 \cdot T_c \cdot \Delta\ell \cdot \mu_{b,NA} \cdot e^{-\mu_t \cdot \ell} \tag{5.1}$$

where S_0 is the source power spectrum and T_c the system coupling efficiency. When $S(\ell)$ is dominated by single backscattered light, μ_t is the attenuation coefficient of the sample and μ_t equals μ_s for non-absorbing samples (this Chapter). The system dependent parameters will be denoted by $\zeta = S_0 \cdot T \cdot \Delta\ell$. The spectra $S(\ell)$ are collected over the detection numerical aperture (**NA**) of the system, therefore we define the measured backscattering coefficient $\mu_{b,NA}$ as the product of μ_s and the phase function $p(\theta)$, integrated over the solid angle of the **NA** in the medium (Section 5.2.3):

$$\mu_{b,NA} = \mu_s \cdot 2\pi \int_{\theta=\pi\text{-}NA}^{\pi} p(\theta) \cdot \sin(\theta) \cdot d\theta \tag{5.2}$$

The terms $\zeta \cdot \mu_{b,NA}$ and μ_s in the single exponential decay model are obtained by fitting a two-parameter (amplitude and decay, respectively) exponential function to $S(\ell)$ vs. ℓ. Uncertainties are estimated by the 95% confidence intervals (c.i.) of the fitted parameters [1]. The model is fitted to the measured $S(\ell)$ starting at $\ell = 50$ µm, up to a path length in the sample of five times the mean free path ($5/\mu_s$ from Mie theory at 480 nm, varying from 100-1950 µm). Prior to fitting the model to $S(\ell)$, a noise level is subtracted from $S(\ell)$, which is the sum of the DC spectra of the sample and reference arm.

Knowledge of ζ is required to calculate $\mu_{b,NA}$ from the fitted amplitude $\zeta \cdot \mu_{b,NA}$. Hereto, ζ is determined in a separate calibration measurement in which $\mu_{b,NA}$ is exactly

known from Mie theory and Eq. 5.2. To this end we used NIST-certified polystyrene spheres of ⌀=409±9 nm (diameter±SD, Thermo Scientific, USA). The obtained ζ was used to determine the $\mu_{b,NA}$ in subsequent measurements.
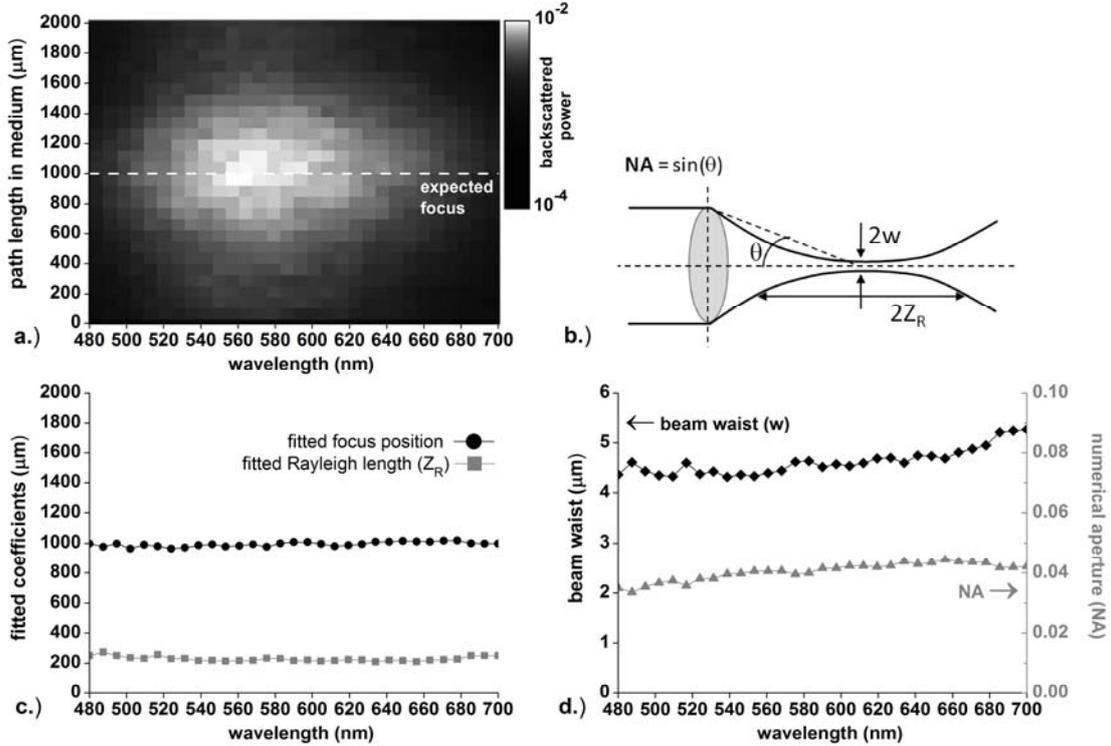

Figure 5.1 *a.) point spread function measurement (**PSF**) on a weakly scattering sample of ⌀198 spheres (0.038 volume%), b.) schematic illustration of focus geometry, c.) fitted focus position (**ℓ_F**) and Rayleigh length (**Z_R**) on the measured PSF, d.) calculated beam waist (**w**) and numerical aperture (**NA**). The parameters **Z_R**, **w** and **NA** are defined within the medium (n=1.35).*

5.2.3   Point spread function

In order to determine the **NA** of our system, we measured the wavelength dependent point spread function (**PSF**) of our system in a weakly scattering medium (0.038 volume% of ⌀198 polystyrene spheres, $\mu_s < 1$ mm^{-1}) and corrected it for the sample's attenuation (Figure 5.1a). The **PSF** can be described by a Lorentzian function [6]:

$$\mathbf{PSF}\left(\ell_F - \ell\right) = \alpha \cdot \left[\left(\frac{\ell_F - \ell}{2\mathbf{Z_R}}\right)^2 + 1\right]^{-1} \tag{5.3}$$

where **α** denotes a scaling factor, **ℓ_F** is the focus position in roundtrip path length units and **Z_R** is the Rayleigh length of the system (Figure 5.1b). Note that the parameter **Z_R** is defined within the medium (n_g=1.35); in air the Rayleigh length is a factor $2n_g$ lower [6].

Fitting this function to the measured PSF results in wavelength dependent values for ℓ_F and Z_R (Figure 5.1c). The fitted ℓ_F agrees well with the expected focus position at ℓ=1000 μm. The fitted Z_R can be used to calculate the beam waist, $\mathbf{w} = (Z_R\lambda/2\pi)^{\frac{1}{2}}$, and from that the **NA** can be derived, using $\mathbf{NA} = \sin(\boldsymbol{\theta}) \approx \sin(\lambda/(\pi\mathbf{w}))$. Figure 5.1d shows that the beam waist is approximately 4.5 μm and the **NA** ranges from 0.035 to 0.045 within the investigated spectral range.

Table 5.1 *Overview of sphere concentrations (volume %) in the investigated samples*

sphere size (diameter ± SD)	monodisperse samples low μ_s (Fig. 5.2)	monodisperse samples μ_s-range (Fig. 5.3 & 5.4)	polydisperse sample (Fig. 5.6)
198±5 nm	-	0.038% to 0.950%	-
409±9 nm	0.071%	0.071% to 0.950%	0.024% &
602±6 nm	0.048%	0.048% to 0.036%	0.033%
799±9 nm	0.038%	0.038% to 0.285%	-
1004±10 nm	0.033%	0.033% to 0.248%	-

5.2.4   Samples and Mie calculations

We prepared a set of four weakly scattering samples, consisting of aqueous suspensions of different sized NIST-certified polystyrene spheres (Thermo Scientific, USA), as indicated in Table 5.1. The sphere concentrations, indicated in volume percentages, were chosen such that μ_s was approximately equal for all samples (~1.5 mm^{-1} at 600 nm). The sphere sizes (ø 409 to 1004 nm) lie within the range of scatterer sizes in biological cells [3]. Calibration of ζ was performed with the 0.071% ø409 nm sample for all sphere sizes and concentrations and a reference measurement on water was obtained to verify the correctness of this calibration.

To test the range of validity of the single exponential decay model for determining μ_s and $\mu_{b,NA}$, it is important to validate the model also for media with higher scattering densities. Therefore, we increased the particle concentration several times for all sphere sizes and included ø198 nm spheres (Table 5.1).

The wavelength dependent oscillations in the $\mu_{b,NA}$ make it possible to derive particle size [3,4,7] and, because of the quantification of $\mu_{b,NA}$ for these LCS measurements, also concentration from a sample for which these properties are unknown. We tested this hypothesis by measuring μ_s and $\mu_{b,NA}$ from a polydisperse sample containing both 409 nm and 602 nm spheres (Table 5.1). To the measured $\mu_{b,NA}$, we performed a multicomponent, linear least-squares fit of the Mie-calculated $\mu_{b,NA}$ of six different sphere sizes (ø99, 198, 409, 602, 799 and 1004 nm) to obtain the individual contribution of all spheres on the measured $\mu_{b,NA}$.

In our Mie calculations, we used wavelength dependent refractive indices of water and polystyrene [8] and integrated over the size distribution of the spheres (2*SD),

given by the manufacturer. Brownian motion of the polystyrene spheres causes Doppler broadening of the measured LCS spectra. For adequate comparison, we convolved the Mie spectra with a Lorentzian, with a line width of 5 to 27 nm, depending on the sphere size-dependent Doppler frequency distribution of the Brownian motion of the spheres, similar to our analysis in Chapter 4 [1].
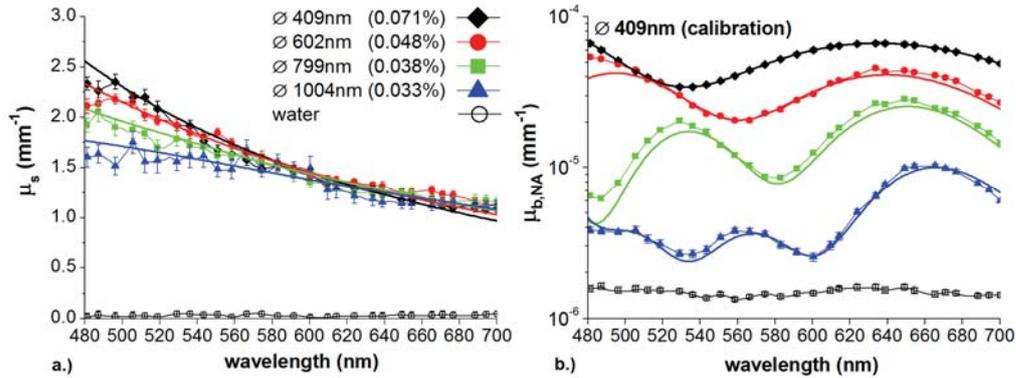

Figure 5.2 LCS (dots) and Mie (thick solid lines) results for (A) scattering coefficients μ_s, and (B) backscattering coefficients $\mu_{b,NA}$ for four aqueous suspensions of different sized polystyrene spheres, and water. Error bars, representing the 95% c.i. of the fitted values, may fall behind data points. The $\mu_{b,NA}$ were calibrated using the 409 nm sample.
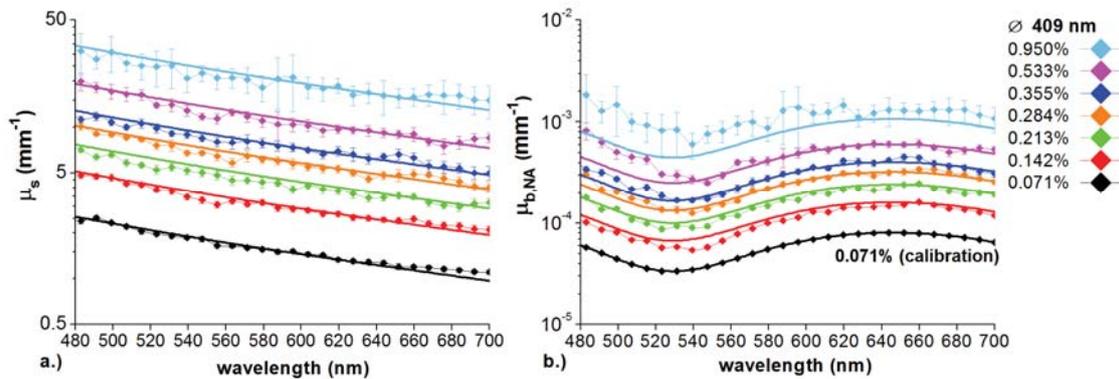

Figure 5.3 LCS (dots) and Mie (thick solid lines) results for a) scattering coefficients μ_s, and b) backscattering coefficients $\mu_{b,NA}$ for six concentrations of 409 nm polystyrene sphere suspensions. Error bars, representing the 95% c.i. of the fitted values, may fall behind data points. The $\mu_{b,NA}$ were calibrated using the 0.071% sample.

5.3   Results and discussion

5.3.1   *Weakly scattering monodisperse media*

Figure 5.2a shows LCS measurements (dots) of μ_s for the four weakly scattering, monodisperse samples in Table 5.1. The LCS measurements agree within 0.2 mm^{-1} with μ_s from Mie theory (thick solid lines) over the entire wavelength range of 480 – 700 nm. The scattering coefficient has a power dependence on wavelength, with different scatter power for different particle sizes. The attenuation coefficient of water is, as expected, ~0 mm^{-1} for all investigated wavelengths.

Figure 5.2b shows the LCS measurements (dots) of $\mu_{b,NA}$ on a logarithmic scale for the polystyrene suspensions. The error bars in this graph are in the same order of magnitude as the marker size. The $\mu_{b,NA}$ differ over an order of magnitude between samples, since the phase function changes considerably with sphere size. The measured $\mu_{b,NA}$ are in excellent agreement with Mie theory (thick solid lines), showing the characteristic sphere size dependent oscillations. The $\mu_{b,NA}$ of water shows no pronounced spectral features, which implies that our calibration method of ζ was applied correctly. We attribute the small differences between measurements and Mie calculations to uncertainties in particle size distribution and refractive index that were used as Mie-input (depending on wavelength, a 1% change in the polystyrene refractive index results in a 11-14% change in μ_s and a 11-25% change in $\mu_{b,NA}$).

5.3.2   *Concentration ranges of monodisperse media*

Figure 5.3 shows the measured μ_s and $\mu_{b,NA}$ for the concentration series of one of the sphere sizes (ø409 nm). The measured μ_s agree with Mie calculations of μ_s within 14%, up to values as high as 34 mm^{-1}, which lies well within the range of tissue scattering (Figure 5.3a). Also the measured $\mu_{b,NA}$ agree well with Mie theory (Figure 5.3b), except for the two highest volume concentrations, where the measurement overestimates $\mu_{b,NA}$ at the shorter wavelengths.

Figure 5.4 shows the measured μ_s and $\mu_{b,NA}$ versus the expected μ_s and $\mu_{b,NA}$ from Mie theory for all sphere sizes at 3 wavelengths within the investigated spectral range: 480, 550 and 700 nm. In general, the measured values agree well with the expected values, but deviations at high concentrations become more apparent for short wavelengths and large sphere sizes. This combination commonly results in an underestimation of μ_s and an overestimation of $\mu_{b,NA}$, which may be explained by the contribution of multiple scattering to the LCS signal. When multiple scattering contributes to the LCS signal, more photons are detected compared to the case of single scattering. As a consequence, the assumption of single scattering in our definition of μ_t in the exponential decay model (Eq. 5.1) is not valid anymore, resulting in the observed overestimation of backscattering ($\mu_{b,NA}$) and an underestimation of attenuation (μ_s). This effect is strongest for large spheres and short wavelengths, since in that case the scattering anisotropy g is largest (Figure 5.5) and hence, multiple scattered photons are more likely to be detected within the **NA** of our LCS system.

The 409 nm concentration series demonstrates that disagreement with the Mie calculated values for the highest volume concentrations is only manifested in $\mu_{b,NA}$ and not in μ_s (i.e. μ_s agrees with the Mie calculated μ_s within the 95% c.i.). For these samples (0.533% and 0.950%), the average surface-to-surface distance between the spheres is

comparable to the wavelength: 760 nm and 556 nm, respectively. Since the effect of multiple scattering would be visible in the measured value of both coefficients, we speculate that another effect may cause this disagreement, i.e. the total scattered field cannot be treated as the superposition of the scattered field by the individual particles (dependent scattering) [9]. Our results indicate that for these sphere concentrations, $\mu_{b,NA}$ is altered to favor more backward than forward directed scattering.
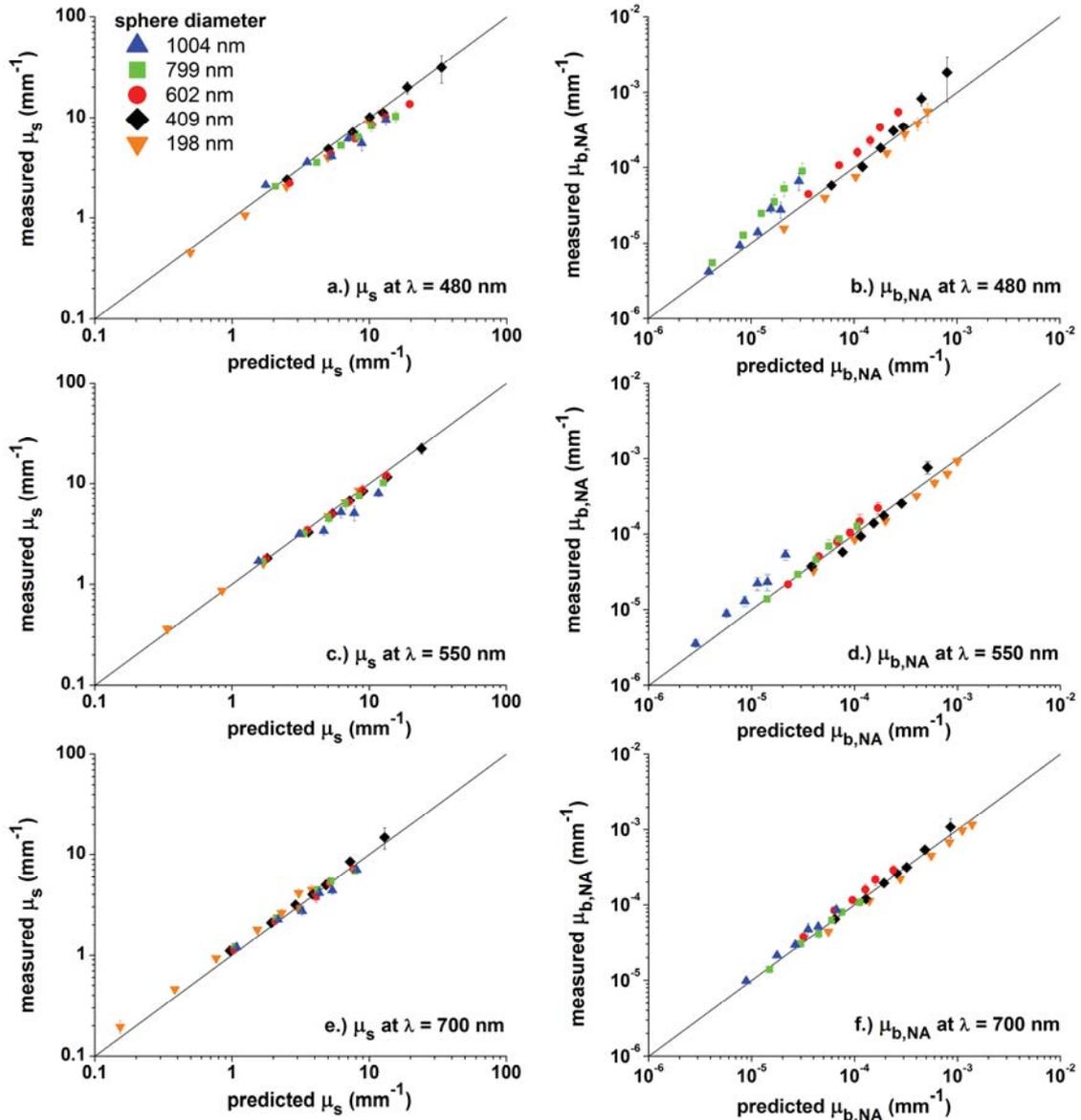

Figure 5.4 *Measured (LCS) versus predicted (Mie theory) values of μ_s and $\mu_{b,NA}$ for 5 sphere sizes (198, 409, 602, 799 and 1004 nm) and various concentrations at 3 wavelengths within the investigated spectral range: 480 nm (a and b), 550 nm (c and d) and 700 nm (e and f).*
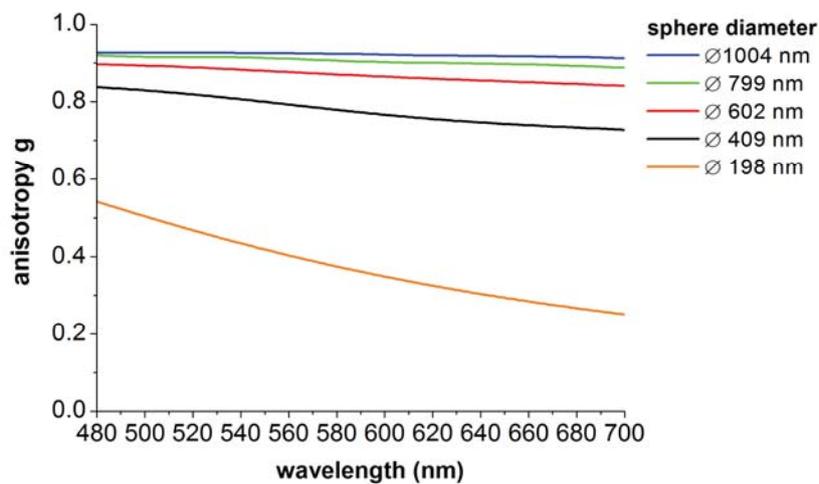
Figure 5.5 *Scattering anisotropies **g** for all sphere sizes, obtained from Mie theory.*

5.3.3   Polydisperse sample

Figure 5.6 shows the measured, Mie calculated and fitted $\mu_{b,NA}$ for the polydisperse sample consisting of two sphere sizes. The measured and Mie calculated μ_s are shown in the inset. The multicomponent fit on $\mu_{b,NA}$ gives a good identification of our sample, as shown in Table 5.2.

The fitted concentration of 602 nm spheres exactly matches the expected concentration and the concentration of 409 nm spheres is underestimated with only 8%. Although not present in the sample, small amounts of 99 nm and 1004 nm spheres contribute to the fit. Please note that the relative contribution of these spheres to the $\mu_{b,NA}$ is low (3% and 9%, respectively) compared to the contribution of the 409 nm (37%) and 602 nm (51%) spheres. We attribute the small differences between measurements and Mie calculations to uncertainties in refractive index and particle size distribution that were used as Mie-input.
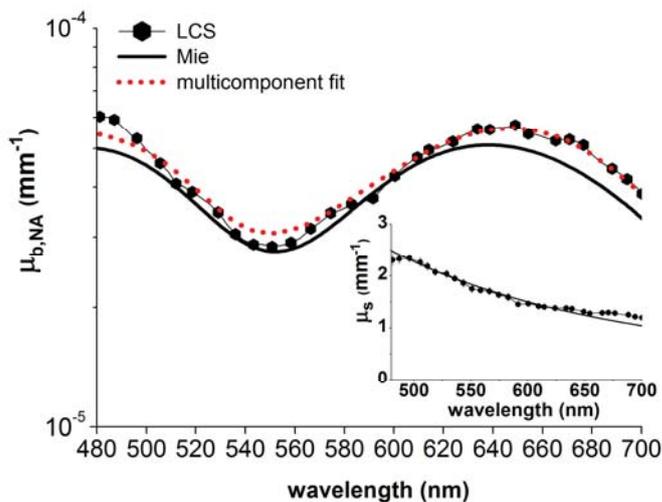

Figure 5.6 *LCS and Mie backscattering coefficient spectrum $\mu_{b,NA}$ for a sample containing both 409 nm spheres (0.024%) and 602 nm spheres (0.033%). Dotted red line: multicomponent fit with 6 sphere sizes on the measured $\mu_{b,NA}$. Inset: LCS and Mie scattering coefficient spectra.*

Table 5.2 *Expected and fitted sphere concentrations*

sphere size (diameter ± SD)	expected concentration (vol%)	fitted concentration (vol%)
99±5 nm	-	0.002%
198±5 nm	-	-
409±9 nm	0.024%	0.022%
602±6 nm	0.033%	0.033%
799±9 nm	-	-
1004±10 nm	-	0.026%

5.4   Conclusion and outlook

The presented results show that LCS enables sample characterization based on absolute values of $\mu_{b,NA}$ and μ_s, the scatter power in μ_s and oscillations in $\mu_{b,NA}$. This very combination of optical properties is characteristic for particle or tissue type [2-7] and therefore offers new opportunities for tissue and/or particle characterization studies. Based on μ_s only, the sphere mix in Figure 5.6 could not have been characterized. In addition, clinical studies have been reported where the measurement of only one parameter was not sufficient to differentiate between tissue types, such as the value of μ_t for measuring (morphological) changes between grades of urothelial carcinoma of the bladder [10]. For these studies, the measurement of both μ_s and $\mu_{b,NA}$ by LCS may assist in better differentiation, because low contrast in μ_s can be accompanied by high contrast in $\mu_{b,NA}$ (Figure 5.1).

In non-absorbing samples, μ_s is extracted directly from the measurement and $\mu_{b,NA}$ requires calibration on a sample with known $\mu_{b,NA}$. To obtain μ_s from tissue, the measured μ_t needs to be corrected for tissue absorption. Several methods to separate μ_s and μ_a from a single attenuation profile have been proposed [11,12]. In addition, the simultaneous measurement of both μ_t and $\mu_{b,NA}$ by LCS may eventually assist in separating scattering and absorption contributions to the LCS signal, since the $\mu_{b,NA}$ is proportional to μ_s but independent of μ_a.

Whereas in this study the scattering properties are measured in non-layered, homogeneous samples, LCS has the potential to measure μ_s and $\mu_{b,NA}$ in individual layers of layered media such as human skin. The controlled path length and the confined measurement volume due to the confocality of the system, in principle allow to measure within a layer of choice, which will be a subject of further study. Even for a confined tissue volume, the $\mu_{b,NA}$ is likely to consist of the contribution of a range of scatterer sizes and it will therefore not exhibit oscillations as clear presented in Figure 5.1, 5.2 and 5.6. Nevertheless, tissue specific spectral features in backscattering have been observed [3,4] and also the absolute value of $\mu_{b,NA}$ contains information on tissue type [2].

Further study is needed to obtain better understanding of the influence of multiple and dependent scattering on the measured μ_s and $\mu_{b,NA}$ for large sphere sizes at high concentrations. Nevertheless, for the smaller sphere sizes (Ø 198 and 406 nm), our results are in excellent agreement with Mie theory up to scattering coefficients as high as 34 mm^{-1}.

In conclusion, we present quantitative and wavelength dependent measurements of scattering and backscattering coefficients from polystyrene sphere suspensions. Our method applies for a broad range of sphere sizes and particle densities, and is in good agreement with Mie theory. LCS measures μ_s and μ_b simultaneously, over a large wavelength range and with good spectral resolution. The combined, wavelength dependent information of μ_s and μ_b is likely to assist in more accurate tissue characterization in tissue optics.

References

1. N. Bosschaart, M.C.G. Aalders, D.J. Faber, J.J.A. Weda, M.J.C. van Gemert, T.G. van Leeuwen, "Quantitative measurements of absorption spectra in scattering media by low-coherence spectroscopy", *Opt. Lett.* **34**, 3746-3748 (2009)
2. J.M. Schmitt, A. Knuttel, R.F. Bonner, "Measurement of optical properties of biological tissues by low-coherence reflectometry", *Appl. Opt.* **32**, 6032-6042 (1993)
3. A.H. Hielscher, J.R. Mourant, I.J. Bigio, "Influence of particle size and concentration on the diffuse backscattering of polarized light from tissue phantoms and biological cell suspensions", *Appl. Opt.* **36**, 125-135 (1997)
4. A. Wax, C. Yang, V. Backman, K. Badizadegan, C.W. Boone, R.R. Dasari, M.S. Feld, "Cellular organization and substructure measured using angle-resolved low-coherence interfometry", *Biophys. J.* **82**, 2256-2264 (2002)
5. A.L. Oldenburg, M.N. Hansen, D.A. Zweifel, A. Wei, S.A. Boppart, "Plasmon resonant gold nanorods as low backscattering albedo contrast agents in optical coherence tomography", *Opt. Express* **14**, 6724-6738 (2006)
6. D.J. Faber, F.J. van der Meer, M.C. Aalders, T.G. van Leeuwen, "Quantitative measurement of attenuation coefficients of weakly scattering media using optical coherence tomography", *Opt. Expr.* **12**, 4353-4365 (2004)
7. C. Ungureanu, A. Amelink, R.G. Rayavarapu, H.J.C.M. Sterenborg, S. Manohar, T.G. van Leeuwen, "Differential pathlength spectroscopy for the quantitation of optical properties of gold nanoparticles", *ACS Nano* **4**, 4081-4089 (2010)
8. S.N. Kasarova, N.G. Sultanova, C.D. Ivanov, I.D. Nikolov, "Analysis of the dispersion of optical plastic materials", *Optical Materials* **29**, 1481-1490 (2004)
9. G. Göbel, J. Kuhn, J. Fricke, "Dependent scattering effects in latex-sphere suspensions and scattering powders", *Waves in Random and Complex Media* **5**, 413-426 (1995)
10. E.C.C. Cauberg, D.M. de Bruin, D.J. Faber, T.M. de Reijke, M. Visser, J.J.M.C.H. de la Rosette, T.G. van Leeuwen, "Quantitative measurement of attenuation coefficients of bladder biopsies using optical coherence tomography for grading urothelial carcinoma of the bladder", *JBO* **15**, 066013 (2010)
11. F.E. Robles, A. Wax, "Separating the scattering and absorption coefficients using the real and imaginary parts of the refractive index with low-coherence interferometry", *Opt. Lett.* **35**, 2843-2845 (2010)
12. C. Xu, D.L. Marks, M.N. Do, S.A. Boppart, "Separation of absorption and scattering profiles in spectroscopic optical coherence tomography using a least-squares algorithm", *Opt. Express* **12**, 4790-4803 (2004)